Line Impedance Estimation

Erik K. Saathoff, *Graduate Student Member, IEEE*, Steven R. Shaw, *Senior Member, IEEE*, and Steven B. Leeb, *Fellow, IEEE*

***Abstract*— Line impedance estimation provides crucial information for power-line communication (PLC), power quality estimation, and grid-connected power electronics applications. Online techniques are particularly useful as the line impedance is time-dependent. This work uses a phase-controlled switch to generate a turn-on transient, which provides information about the line. Previous switching-based approaches focus on fitting line characteristics to a model. This article extends previous work by using a common electrical load in place of previously used capacitors, inductors, and short circuits. Nonparametric line impedance estimation is also demonstrated. An inrush transient generates a current with a wide-bandwidth spectral content to replace a sinusoidal injection sweep. Good estimation performance is demonstrated from dc up to 200 kHz.**

***Index Terms*— Estimation, impedance measurement, prediction methods, system identification, transfer functions.**

I. Supply Impedance

From a service connection, an electric utility, ac or dc, can be modeled as a source in series with an impedance. The impedance exerts a critical influence on the effective behavior of the service connection. For example, line impedance determines the available fault current. Load currents flow through the line impedance, creating series voltage drops that affect the power quality by introducing droop and harmonic distortion in the delivered voltage waveform. Line impedance may be a critical factor in determining inrush current to a load and, therefore, essential in properly designing or setting protection circuitry to avoid nuisance tripping. High-quality measurements of the line characteristics are important for the design of reliable power-line communication (PLC) transceivers [1]. Line measurements also aid in the determination and optimization of PLC channel capacity for power-constrained PLC systems [2], [3]. Characterization of line impedance may also be important for the design and control of grid-connected power electronics.

A wide variety of techniques have been proposed and explored to characterize line impedance. Beattie and Matthews [4] present a technique to determine the *R–L* impedance model of the electrical utility by connecting a capacitor to the line at a fixed point in the line cycle. Each test provides information on the apparent inductance and resistance. The resulting model is used to predict line voltage distortions caused by other current transients. Shaw *et al.* [5], [6] expand on this technique with a programmable capacitor to generate different oscillation frequencies. This approach creates a sweep of test frequencies for estimating the frequency-dependent resistance of the utility wire. Some line model extraction techniques make use of inductive loads. The commutation time in a line commutated converter can be used to determine the inductance of the line [7]. An improvement on this technique uses an inverter to drive harmonic currents onto the line [8]–[10]. Matsui *et al.* [9] extend beyond and usual *R–L* model by investigating the line capacitance as well. Even a short circuit has been demonstrated as a tool to measure line impedance [11].

Line impedance is frequency-dependent due to parasitic reactive elements. Fewer techniques for measuring frequency-dependent line impedance are available, and these techniques can be more time-consuming and invasive. For example, by connecting a high-pass coupler to the line, sinusoidal currents can be injected and the associated voltage measured [12]–[17]. Line impedances at low frequencies may be comparable to parasitic impedances introduced by the coupling technique, making full-spectrum measurements a challenge.

"Smart" utility connections with solid-state controls offer interesting opportunities, likely to become more prevalent, for probing line impedance once or more frequently. Line impedance estimates can be used to estimate available short circuit fault currents, power quality, and inrush current. This article demonstrates the estimation of line impedance over a wide frequency range using a phase-controlled switch [18] and a "common" load that might be connected to a smart switch, light dimmer, or other power electronic interfaces. The switch employed in the experiments presented here is built using TRIACs. It provides a single turn-on event every half line cycle. By changing the turn-on phase angle of the connected load, a variety of inrush transients can be generated. These currents provide ample spectral content to characterize the line impedance over a range of frequencies. Techniques presented in this article expand on [5] and [6] by employing a common load instead of a test capacitor. Since an inrush current is used, as opposed to a frequency sweep of injected currents, the entire test is completed quickly with a single "turn-on" test event. The approach presented in this article does not require line frequency rejection and also does not require careful control or characterization of coupler parasitics.

Manuscript received August 7, 2020; revised October 10, 2020; accepted October 26, 2020. Date of publication November 20, 2020; date of current version January 4, 2021. This work was supported in part by The Grainger Foundation and in part by the Cooperative Agreement between the Masdar Institute of Science and Technology (Masdar Institute), Abu Dhabi, United Arab Emirates, and the Massachusetts Institute of Technology (MIT), Cambridge, MA, USA, under Reference 02/MI/MIT/CP/11/07633/GEN/G/00 and by the MIT-Indonesia Seed Program. The Associate Editor coordinating the review process was Guglielmo Frigo. *(Corresponding author: Erik K. Saathoff.)*

Erik K. Saathoff and Steven B. Leeb are with the Department of Electrical Engineering and Computer Science, Massachusetts Institute of Technology, Cambridge, MA 02139 USA (e-mail: saathoff@mit.edu; sbleeb@mit.edu).

Steven R. Shaw is with the Department of Electrical and Computer Engineering, Montana State University, Bozeman, MT 59717 USA (e-mail: sshaw@montana.edu).

Digital Object Identifier 10.1109/TIM.2020.3039642

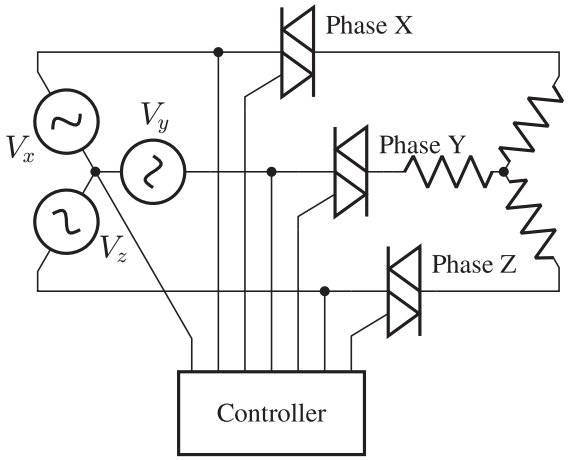

Fig. 1. Three-phase diagram of the source, switch, and load.

Section II of this article provides an overview of the phase-controlled switch hardware used for testing. Section III describes a signal processing operator-substitution method for parametric impedance estimation (PIE), with an experimental demonstration presented in Section IV. Section V discusses a non-PIE (NPIE) approach based on the empirical transfer function estimate (ETFE), with experimental results demonstrated in Section VI.

II. Smart Switch

Fig. 1 presents a simplified schematic of the TRIAC-based phase-controlled switch used to demonstrate the signal processing techniques presented in this article. This switch is presented and deployed here to demonstrate the line impedance estimation algorithms. A variety of "smart switch" devices could be used to probe line impedance. This switch can be used for either three-phase loads or an arrangement of single-phase loads. The semiconductor power devices introduce some nonidealities due to voltage drop, incremental resistance, parasitic series inductance, and gate drive dynamics. Although these effects can slightly distort the inrush current drawn by a load, the techniques presented here for line impedance estimation are unaffected provided that the current and voltage retain sufficient excitation to characterize the line impedance. The approaches demonstrated here can be extended to other semiconductor switch arrangements, including MOSFETs and GaN FETs. Other types of switches may reduce parasitic effects compared with the TRIAC and provide additional test behavior, including the possibility of easily achieving multiple turn-on and turn-off events within a line half-cycle.

Fig. 2 shows an annotated view of the switch hardware. Each TRIAC is controlled by a Cypress Semiconductor PSoC 5LP microcontroller through galvanically isolated signal interfaces. A polarity detector reports whether the phase voltage is above the neutral and the microcontroller uses this to time the turn-on event for any of the phases. Especially, the turn-on phase angle is defined starting at the positive-slope zero-crossing of the line voltage. A positive-edge-triggered

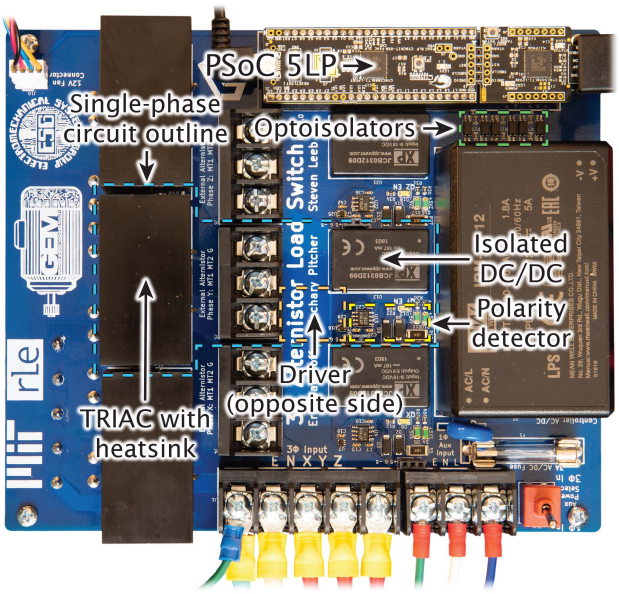

Fig. 2. Annotated view of the PCB.

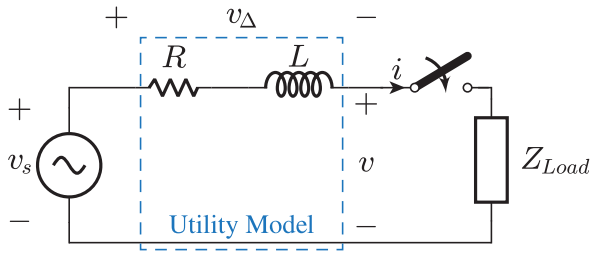

Fig. 3. Circuit model for the parametric line impedance estimation.

delay counter in the microcontroller connected to the polarity detector performs the timing in increments of 250 ns.

III. PIE: Theory

Fig. 3 shows a single-phase ac utility connection as an example, characterized by resistance R and inductance L. The resistance and inductance can be extracted from measurements of sufficiently information-rich voltage and current waveforms. The model voltage source is assumed as time-shift invariant. That is, in practice when estimating line impedance, the utility voltage is assumed quasi-static for several line cycles to permit testing. Multiple samples may be taken and outliers discarded if conditions in the circuit or utility operation change. A discussion on how to remove such outliers and their expected impacts on results is provided at the end of Section V.

Fig. 4 illustrates the setup for an estimation technique that uses the inrush current of a load to identify line impedance. To estimate line impedance, a cycle of the utility waveform is sampled and saved as an exemplar prior to connecting the load. In the immediate next cycle, the phase-controlled switch connects a load to the utility connection, as shown in Fig. 3. The voltage v and current i at the connection to the utility are sampled during the transient test. Subtracting the pretransient cycle data from the transient cycle data yields the voltage

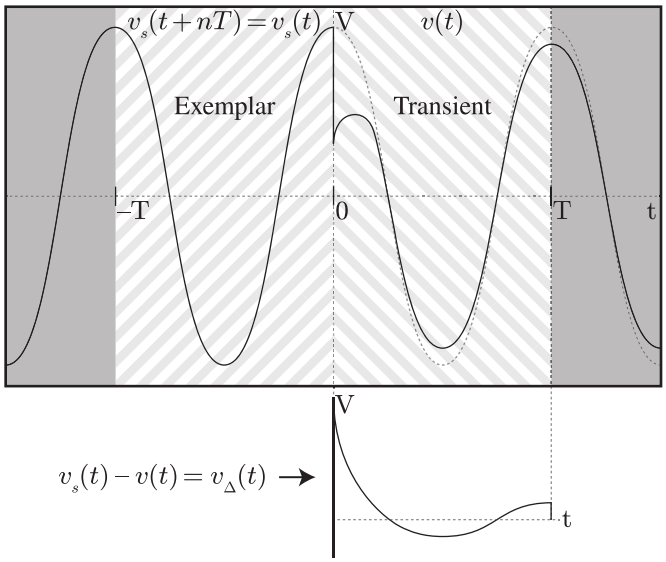

Fig. 4. Typical utility voltage waveform containing the exemplar and transient data segments.

difference v_Δ that approximates the voltage across the line impedance during the inrush time interval.

This circuit is described by the KVL relationship

$$v_s(t) - v(t) = v_\Delta(t) = (R + Lp)i(t) \tag{1}$$

where p is the time derivative operator. The measurements of voltage, current, and the derivative of current could be used to set up a least-squares tableau in order to solve for the parameters R and L. This approach requires formulating the derivative of a measured waveform and becomes more challenging and noise-prone as higher order derivatives are computed for more complex systems. The operator-substitution method uses filtered waveforms, avoiding the need to compute derivatives [19]. This method is also referred to as the "lambda method."

Equation (2) defines the λ operator. This operator, when acting on a signal, computes the response of a first-order low-pass filter with time constant τ acting on the signal

$$\lambda = \frac{1}{1 + p\tau}. \tag{2}$$

The time derivative operator p can, therefore, be expressed as

$$p = \frac{1 - \lambda}{\lambda\tau}. \tag{3}$$

Substituting (3) into (1) and eliminating λ in the denominator yield

$$\tau R[\lambda i](t) + L\Big(\big(i(t) - [\lambda i](t)\big)\Big) = \tau[\lambda v_\Delta](t). \tag{4}$$

This equation can be reformed as

$$-\frac{R}{L}[\lambda i](t) + \frac{1}{L}[\lambda v_\Delta](t) = \frac{1}{\tau}\Big(i(t) - [\lambda i](t)\Big) \tag{5}$$

and replicated to obtain an overconstrained system in the parameters (R/L) and $(1/L)$, as follows:

$$\begin{bmatrix} -[\lambda i](t_1) & [\lambda v_\Delta](t_1) \\ -[\lambda i](t_2) & [\lambda v_\Delta](t_2) \\ \vdots & \vdots \\ -[\lambda i](t_N) & [\lambda v_\Delta](t_N) \end{bmatrix} \begin{bmatrix} \widehat{\frac{R}{L}} \\ \widehat{\frac{1}{L}} \end{bmatrix} = \begin{bmatrix} \frac{1}{\tau}\Big(i(t_1) - [\lambda i](t_1)\Big) \\ \frac{1}{\tau}\Big(i(t_2) - [\lambda i](t_2)\Big) \\ \vdots \\ \frac{1}{\tau}\Big(i(t_N) - [\lambda i](t_N)\Big) \end{bmatrix}. \tag{6}$$

In implementation, the λ operator is calculated at times $t_n = n\Delta t$ on an array of N voltage and current samples. The notation $[\lambda i](t_k)$ indicates the k'th value of the filtered $i(t)$. Since λ is a continuous-time operator, it is important to use finely sampled data to reduce the time quantization error.

Finding a least-squares solution for (6) provides estimates for the line inductance and resistance. In (6), the system has been arranged so that the regressors are filtered. This reduces bias in the estimates that may result from the accumulation of measurement-noise variance terms if the system is solved via ordinary least-squares. The effects of noise in this technique are discussed in [19].

This approach for estimating R and L uses only the input terminal voltage and current into the phase-controlled switch. The technique does neither depend on the parasitics of the switch nor the characteristics of the chosen load, which may be nonlinear, as in the case of resistance with a thermal coefficient.

IV. PIE: Demonstration

To demonstrate the "lambda method" PIE technique as an application of the phase-controlled switch, the impedance of a 30.5-m (100-ft) section of single-phase utility cable is estimated. In these experiments, the phase-controlled switch connects a 250-W incandescent lamp to a utility connection at a variety of different phase angles, with and without an extended section of utility wiring upstream from the switch. The testing is carried out over a long time period so that the load cools completely between tests. Especially, the load is OFF for 3 min between tests. The lamp is switched ON for approximately 50 ms to minimize the thermal energy retained by the lamp. This procedure ensures that the filament is in thermal equilibrium with the environment at the start of each test.

Multiple tests are run at each phase angle, α, to check for consistency. One test is performed at each of the desired phase angles. The sweep of phase angle tests is repeated to build a full data set. This protocol distributes the effects of drift across each phase angle's associated data.

For each set of waveform data captured, a section with the length of one full line cycle is used for computation with (6). The preceding cycle is used as the exemplar of the source voltage, which is used to find the transient voltage drop over the line impedance, i.e., the examplar and transient voltage cycles are adjacent in time. In this example, τ is set at 1 μs.

The results of the inductance estimation are shown in Fig. 5(a) for estimates with and without the single-phase utility

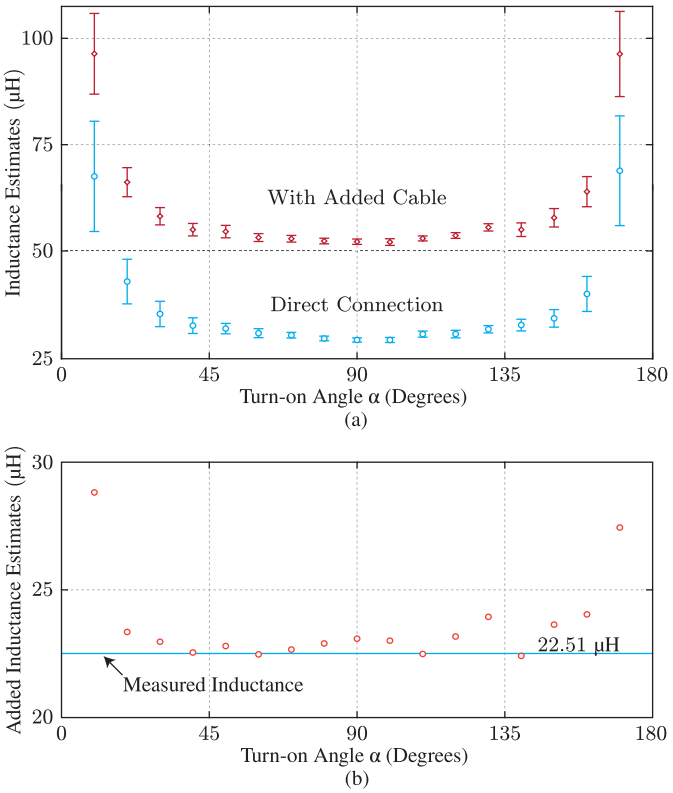

Fig. 5. (a) Average line inductance estimates for various turn-on angles with or without an added single-phase utility cable with $\pm\sigma$ error bars. (b) Average line inductance of the utility cable for various turn-on angles.

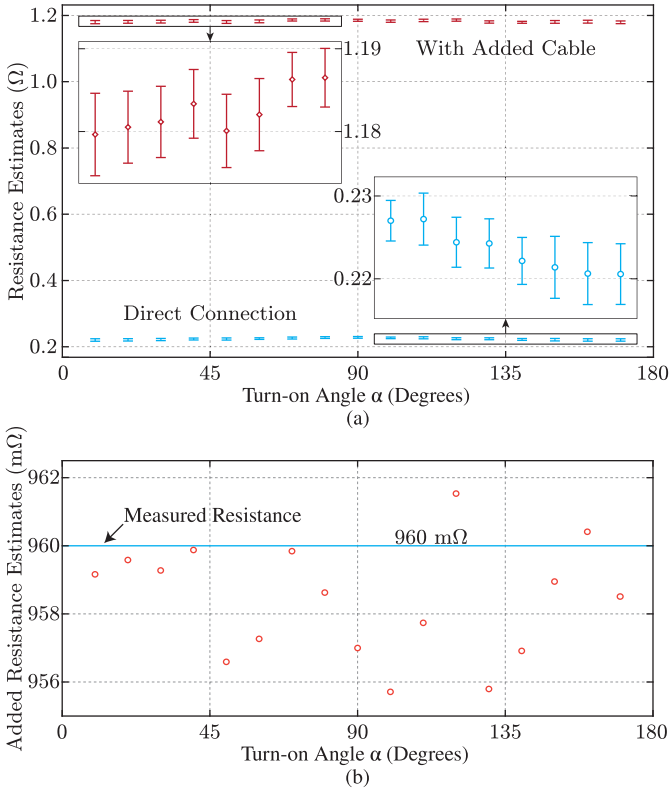

Fig. 6. (a) Average line resistance estimates for various turn-on angles with or without an single-phase utility cable with $\pm\sigma$ error bars. (b) Average line resistance of the utility cable for various turn-on angles.

cable. In the range of 40°–140° voltage phase angle, the estimates are similar, and the standard deviation is low. The difference between the two inductance estimates represents how much inductance the single-phase utility cable adds and is shown in Fig. 5(b). The flat line at 22.51 μH shows the actual inductance of the added utility cable measured with an LCR meter. The match between the estimate and the real value demonstrates the effectiveness of this approach. Note that, as the test phase angle approaches integer multiples of 180°, i.e., as the turn-on occurs closer to a voltage zero crossing, the standard deviation increases, and the average value drifts. Excitation is relatively low at these phase angles, and noise dominates the system identification problem. A practical application for line impedance estimation would avoid these test phase angles to ensure a reliable data set.

Fig. 6(a) shows resistance estimates with and without the added single-phase utility cable. Here, the variance in the resistance values remains consistent over the entire range of firing angles, and the averages are roughly consistent. The difference between the estimates with and without the utility cable closely matches the impedance analyzer estimate of the cable, as shown in Fig. 6(b). The line plotted at 960 mΩ is the dc resistance of the wire, which is essentially unaffected by skin effect or other frequency-dependent effects through approximately 10 kHz.

Accurate results depend on accurate measurement of the service voltage and line current. For example, the current clamp must be calibrated for zero offsets. The offset in the voltage measurement matters less since the "lambda method" is driven by differences in voltage measurements, not absolute voltage measurements.

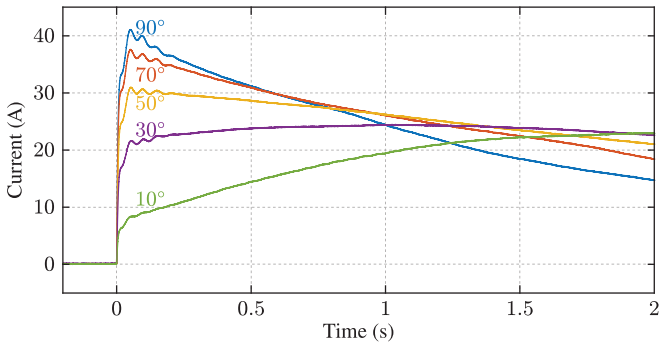

Fig. 7. Inrush currents observed at various turn-on angles.

The error in the inductance estimate for turn-on times near zero-crossings can be further explored by examining (1). In effect, the least-squares estimation method is attempting to find which values of R and L that best solve this equation for all data points. As shown in Fig. 7, as the firing angle approaches an integer multiple of 180°, the initial current inrush becomes smaller in comparison to peak inrush near 90°. At the extreme of a zero-crossing turn-on, the incandescent lamp has no sharp transient currents. The inrush becomes a slow transient on the order of a few milliseconds. Taking the time derivative of the current, in this case, only provides values near zero, but the overall magnitude of the current during

the turn-on transient does not change significantly, that is, the data are insufficiently rich to support the two-parameter identification when taken close to zero crossings of the line voltage and cause a loss of rank. This loss of rank can also occur by choosing τ incorrectly. The value should be selected such that $(1-\lambda)$ is not zero and λ is not one, which corresponds to τ being either too slow or too fast, respectively. Conveniently, this selection is performed in postprocessing and can be adjusted as needed.

When the amplitude of current dominates over the amplitude of the time derivative of the current, (1) acts as a resistance estimator. The estimate of L has less effect on the overall solution and varies around a dominating estimate of resistance. Thus, the variance and average values of the L estimate become unreliable. The level of current does not change significantly over the range of currents. The consistent importance of R in (1) makes the estimate repeatable, and the resulting resistance estimate is relatively flat across the range. A small variation is expected as the equation changes to better fit a resistance value to the data.

To obtain better results, we could: 1) crop out data with low (di/dt) to increase the average amount of useful information for the inductance estimate; 2) use capacitors as a load as the ringing will interact heavily with the line inductance as used in [4]–[6]; and 3) use switching to increase the number of current steps possible as a TRIAC can only generate one step per half-cycle. This last option becomes possible with a new version of the load switch implemented with MOSFETs or other fully controllable devices.

V. NPIE: Theory

Rather than fitting a predefined model to an observed grid interaction, NPIE can be performed to gain additional insight into the details of the grid connection. Using the ETFE [20]–[22], the line impedance as a function of frequency can be extracted from an inrush-transient perturbation. The generated impedance frequency spectrum facilitates the selection and fitting of an optimal line model.

The ETFE, as shown in (7), is the ratio of the Fourier transforms of the input and output of a system

$$G(\omega) = \frac{Y(\omega)}{U(\omega)}. \tag{7}$$

A discrete Fourier transform (DFT) converts the sampled data into the frequency space

$$Y(\omega) = \Delta t \sum_{n=-\infty}^{\infty} y(n) e^{-j\omega t_n}$$
$$t_n = n\Delta t. \tag{8}$$

Restricting $y(n)$ to be zero everywhere except inside some sampling interval, the DFT can be rewritten as

$$Y(\omega) = \Delta t \sum_{n=0}^{N-1} y(n) e^{-j\omega t_n} \tag{9}$$

where N is the number of samples taken and the time interval of the captured data is $\Delta t(N-1)$. A system with a current input and voltage output is described by some impedance function. Plugging (9) into (7) and using the definitions of v_Δ and i from Section IV, the line impedance becomes

$$Z(\omega) = \frac{V(\omega)}{I(\omega)} = \frac{\sum_{n=0}^{N-1} v_\Delta(n) e^{-j\omega t_n}}{\sum_{n=0}^{N-1} i(n) e^{-j\omega t_n}}. \tag{10}$$

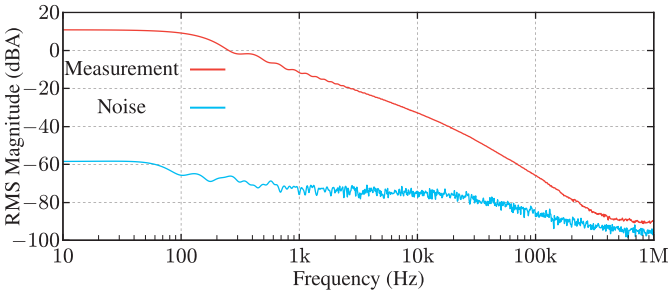

Fig. 8. DFT of a current sample during a transient and with no current to represent the noise floor.

Since this technique will be used on nonperiodic waveforms, it is important that v_Δ and i are zero outside the sampling interval. Simply capturing the inrush transient is equivalent to applying a rectangular windowing function, and the resulting frequency-domain convolution produces incorrect estimates. During data capture after the switch is turned off, the current must return to zero and the voltage to its sinusoidal steady-state value.

When a division by zero occurs in (10), the output must be considered undefined. In a practical system, the problem of division by zero is replaced by noise dominating the DFT. The overall measurement noise resulting from the probe, data acquisition unit, quantization, and round-off error limits the minimum signal level that can be reliably measured. Since any transient other than a perfect impulse decays with higher frequency, it is not possible to perform the ETFE at arbitrarily high frequencies. Fig. 8 demonstrates this phenomenon by showing the noise floor of the current measurement and the DFT of a typical inrush current transient. Reliable performance and low variance have been observed with at least 10 dB of separation between the signal and the noise floor. Even with good SNR, singularities can occur, but these points can be removed [23].

To produce high fidelity results, the following algorithm is used: 1) perform the ETFE on many transient data sets; 2) ignore frequencies where the rms magnitude checked over many DFT results is not at least 10 dB above the rms noise floor; 3) average the impedance results across the various data sets while ignoring points where an individual DFT point falls below the rms noise floor; and 4) apply a smoothing operation with an adaptive Hamming window. By making the window bandwidth proportional to the frequency of interest, the smoothing operation maintains optimal performance at high frequencies without obscuring low-frequency data. The bandwidth should be chosen to smooth out the ETFE as much as desired without appreciably distorting the result. Based on empirical testing, the total bandwidth of the window is set to $\Delta\omega = 0.6\omega_o$, where ω_o is the frequency of interest that slides across the frequency range. This operation can be conducted

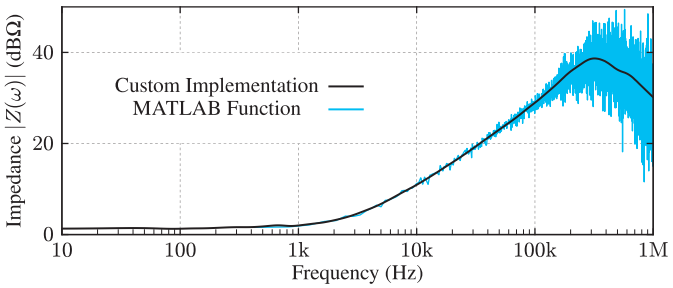

Fig. 9. Comparison between the presented ETFE algorithm and the built in MATLAB ETFE function.

with only one transient data set, but the use of many data sets will provide cleaner results and permit the calculation of a trustworthy standard deviation.

MATLAB provides an ETFE function. While it does have built-in smoothing functionality, the bandwidth does not change with frequency, and thus, the smoothing cannot be optimized to work at both low and high frequencies. Furthermore, the DFT results cannot be evaluated, and thus, the process for trimming out poorly excited data cannot be performed. Despite the diminished utility of the built-in function, the mean should be consistent with the presented algorithm. Fig. 9 shows a typical impedance estimate using both the stated algorithm and the MATLAB ETFE function. These plots are reasonably consistent and verify that the custom algorithm agrees with existing methods.

It is common practice to use a fully nonparametric approach, such as the ETFE, to obtain modeling insight and fit models to the ETFE. As the primary approach is nonparameteric, these are collectively referred to NPIEs in the following.

As with PIE, the calculation of v_Δ requires the model voltage source to be time-shift invariant. Since T is assumed to be the ideal line period, slow frequency variations will cause imperfect "carrier" cancellation. A phase error of $2\pi(\Delta f/f_o)n$ between the exemplar and transient data segments accentuates some low-frequency harmonics. Depending on the sign of Δf, the nonparametric impedance estimate at and above line frequency will increase or decrease. The width of this error will be limited by the existence and magnitude of harmonics in the grid voltage. It is likely that lower frequency errors will affect the value of R more than L. Slow voltage variations are not a problem since the exemplar and transient data segments are captured in neighboring line cycles. However, faster voltage transients from sources, such as lightning and capacitive load disconnection [24], [25], will cause large distortions in both PIE and NPIE.

Fortunately, the mitigation of line events is relatively easy for slow changes. Frequency variations generally occur on the time scale of seconds for grids with high inertia [26], [27]. By measuring the line frequency [28]–[30] and adjusting the data processing accordingly, off-nominal tests can still be used. For faster changes, two techniques can screen out the majority of bad tests. First, the measurement system can capture an extra period before the exemplar and take the difference between the two. If the system finds a large enough difference, then the chosen line period is potentially varying

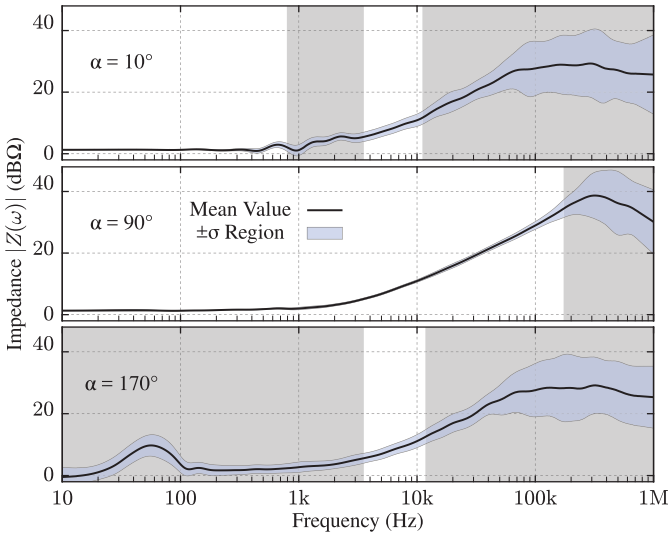

Fig. 10. Line impedance of the single-phase utility cable and electric utility at various turn-on angles α. The test load is a 250-W incandescent bulb.

or indicating that there is some other voltage instability on the line, which would invalidate the test. In this case, the test can be delayed or discarded as appropriate until the line stabilizes. The second mitigation technique requires the test load to have a consistent inrush waveform and that the line frequency and voltage are nominal. The test system can compute v_Δ and i, as would normally be fed into (6) and (10), average several tests, and discard any results that deviate significantly from the average. This averaging approach eliminates quick transients that occur just after the exemplar is captured. Using all these mitigation techniques together makes variability due to line events unnoticeable in the experimental results.

VI. NPIE: Demonstration

To verify the NPIE technique, the impedance estimate of the electric utility with the 30.5 m (100 ft) single-phase utility cable is generated and compared with the results from the PIE. For these transient tests, a 250-W incandescent bulb is used at a variety of turn-on angles, α, from 10° to 170°. The sweep of angles is repeated multiple times to distribute the effects of drift across each phase angle's associated data. The technique for finding v_Δ is the same as in Section III, but the switch is reconfigured, so the TRIAC is driven until the next zero-crossing occurs. The switch will be OFF for more than half the captured transient period. The utility voltage v will have sufficient time to settle back to the exemplar v_s inside the transient window and will permit the use of (10).

Fig. 10 provides an overview of the impedance magnitude calculated using (10) with 100 samples taken at each phase angle. The range of α from 40° to 140° provides extremely similar results, so the 90° test is shown to represent this range. Outside this range, the mean impedance starts to become distorted, and σ increases. The worst case angles of 10° and 170° are shown, as they deviate the most from the behavior of the rest of the test angles. The grayed out sections of the plots indicate frequencies that have a poor SNR.

From the figure, it is clear that the *R–L* line impedance model is reasonable for low frequencies. Above 300 kHz, the effect of line capacitance becomes apparent as it changes the slope of the impedance to −20 dB/decade. The *R–L* line impedance model is incomplete, and the impedance plot makes it clear that a capacitive branch must be added to the model. The new model can then be fitted to the generated line. However, the frequencies above 200 kHz always fail the SNR test, so the model will not be fitted to this part of the data.

The two extreme cases of 10° and 170° each demonstrate a limitation to this approach. For 10°, the inrush transient is significantly smaller and slower and results in less high-frequency content. The current SNR drops and causes unreliable results at a lower frequency than with 90°. However, this test angle has the longest ON-time, which provides the most information about the lowest frequencies and, thus, a very small standard deviation.

The 170° case also has degraded performance at high frequencies due to the inrush being small. This test angle has the shortest ON-time, resulting in less than 3% of the sampling interval containing nonzero current. When the ON-time becomes significantly smaller than the sampling period, the DFT will be more susceptible to noise and results in poor accuracy and standard deviation. The two effects at high and low frequencies result in poor SNR and variance over most of the 170° test.

The 90° case has excellent performance over most of the frequency range but, eventually, struggles at high frequencies due to the low excitation level in this frequency range. The use of different loads cannot completely overcome this limitation as loads that can produce high frequencies, such as small value capacitors and smaller and shorter current transients. A change of topology to a switch that can be turned on and off multiple times in a single line half-cycle would be a better approach to generating a wide-bandwidth current perturbation.

To test the effect of current harmonics generated by a load on line impedance estimation, the incandescent bulb was replaced with a 5-W LED light with no other modifications to the measurement setup. The LED light connects to the line with a full-bridge rectifier feeding a 22-μF capacitor in parallel with the LED strings. Fig. 11 provides an overview of the impedance estimation results using the new test load. This load was chosen to display the effectiveness of NPIE with a nonlinear power-electronic load. Mindful of the significantly lower load power level, the 10° and 170° tests were replaced with 20° and 160°. The mean values from the incandescent bulb tests for 20°, 90°, and 160° are also plotted for comparison purposes. The results are very close to those captured with the incandescent bulb. In essence, across a range of α where the excitation provided by the load is significant, the precise nature of the load is not relevant for the accuracy or precision of the line impedance estimation. This is consistent with the method's mathematical formulation. The load current essentially becomes a current source driving the identification method. Any sufficiently rich load current will lead to good estimation results.

Fig. 12 matches the *R–L* model to the impedance frequency spectrum generated for the 90° case with the values of the model given in Table I. The fitting only considers frequencies below 170 kHz, as the low SNR data should not be incorporated into the model. The values from PIE at the same turn-on angle are given in Table II. These values are very similar and demonstrate the effectiveness of the NPIE approach.

To present another example for a line impedance result, a 1-μF-film capacitor is connected directly to the line in

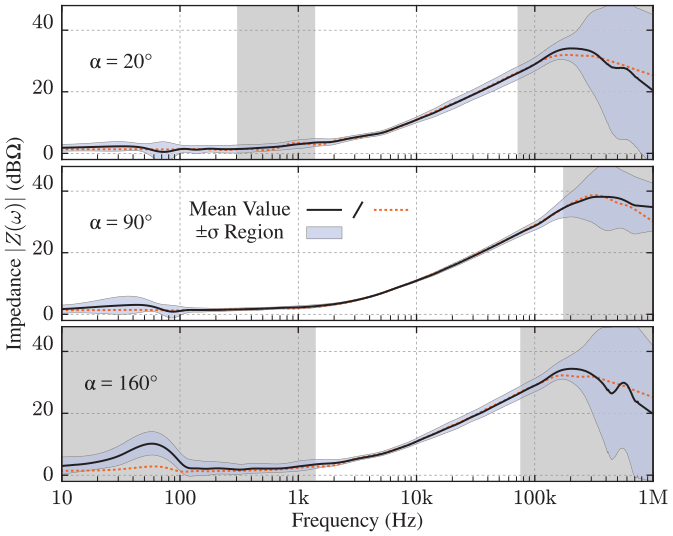

Fig. 11. Line impedance of the single-phase utility cable and electric utility at various turn-on angles α. The test load is a 5-W LED light. The mean values from the incandescent bulb tests are included as dashed lines.

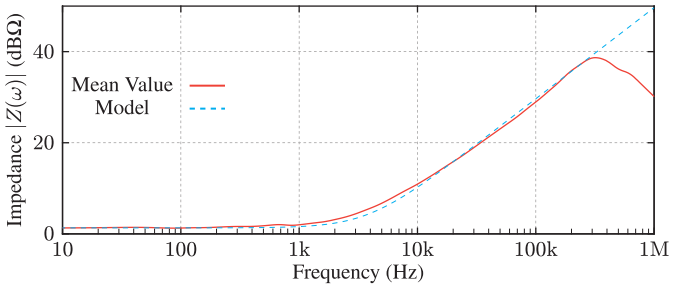

Fig. 12. Line impedance of the single-phase utility cable and electric utility. The impedance of a fitted *R–L* model is also shown.

TABLE I

R–L LINE IMPEDANCE PARAMETERS FROM THE NPIE METHOD

Parameter	Value
L	48.4 µH
R	1.16 Ω

TABLE II

R–L LINE IMPEDANCE PARAMETERS FROM THE PIE METHOD

Parameter	Value
L	52.2 µH
R	1.19 Ω

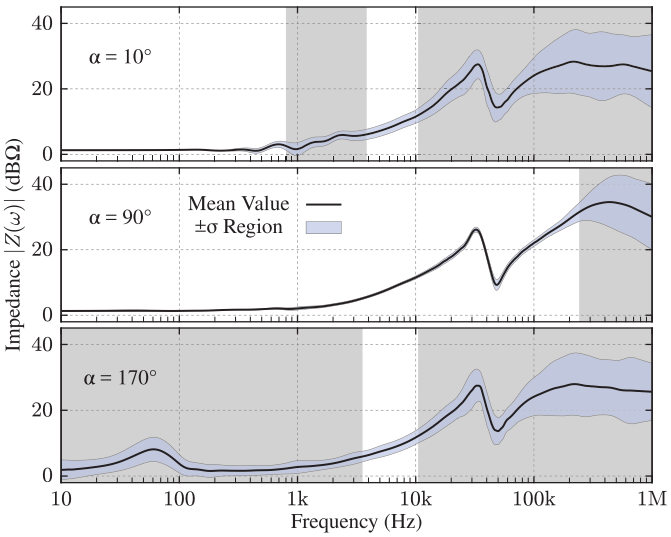

Fig. 13. Line impedance of the single-phase utility cable and electric utility with the added phase X capacitor at various turn-on angles.

parallel at the connection between the electric utility and the single-phase extension cable. The capacitor is connected from line to neutral on the same electrical phase as the switch (phase X). The testing and data analysis from the case without the capacitor is repeated exactly. This situation is not atypical, as many EMI filters make the same capacitor connection to the line with hundreds of nanofarads. Large power supplies may even exceed the 1 μF used here.

Fig. 13 shows the new results for the impedance frequency spectrum. Here, the smoothing bandwidth is decreased by a factor of five in areas with a high second derivative to prevent distortion of the results. For every turn-on angle, a large inflection has appeared centered near 40 kHz, but all other characteristics of each plot are the same. The new feature is indicative of an R–L section that becomes shunted by a capacitor at a sufficiently high frequency. The impedance continues to increase shortly after indicating that the connection to the capacitor has parasitic inductance. Thus, a logical new model would add an RLC branch to the original R–L model. One could also create a more intuitive model that corresponds to discrete elements, as shown in Fig. 14. Here, R_1 and L_1 represent the R–L characteristics of the electric utility, and R_2 and L_2 represent the same for the added utility cable. R_3, L_3, and C represent the capacitor with parasitics.

Now that NPIE has aided in the selection of a line impedance model, the model can be fit to the frequency response. Fig. 15 shows the new higher order model fitted to the data from the 90° case, and the resulting parameters from the model are given in Table III. Again, the model matching software ignores the frequencies above 170 kHz. The series inductance and resistance, $L_1 + L_2$ and $R_1 + R_2$, are given as well and correspond well with the values obtained from the PIE as expected. Furthermore, L_2 is close to the measured inductance of the single-phase utility cable, and C is reasonably close to the real value of 1 μF. R_2 does not match well with the expected value of 960 mΩ, but forcing R_2 to be this value in the fitter still provides an acceptable match.

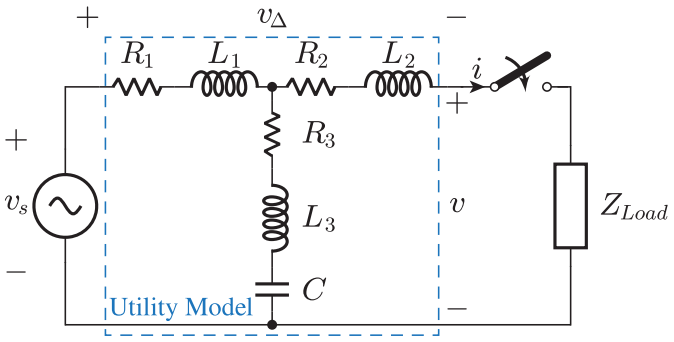

Fig. 14. Circuit model for the higher order line impedance estimation.

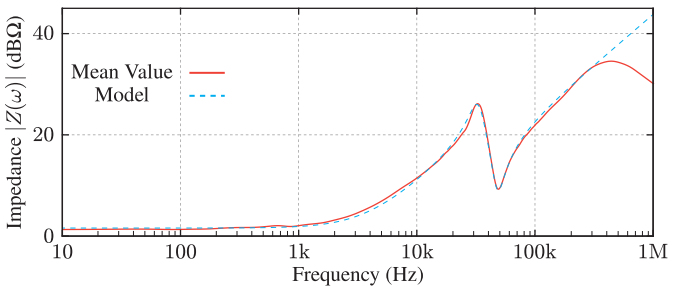

Fig. 15. Line impedance of the single-phase utility cable and electric utility with the added phase X capacitor. The impedance of a fitted higher order model is also shown.

TABLE III
HIGHER ORDER LINE IMPEDANCE PARAMETERS

Parameter	Value
L_1	27.2 µH
L_2	24.6 µH
L_3	84.3 nH
R_1	1.16 Ω
R_2	41.4 mΩ
R_3	573 mΩ
C	836 nF
$L_1 + L_2$	51.8 µH
$R_1 + R_2$	1.20 Ω

The chosen model does not perfectly match the true behavior of the system, so physically identifiable parameters may not take the expected values to obtain the best fit. A model that characterizes the observed data well is still extremely useful.

Different capacitor connections present different results in the spectral analysis. The case of a single-phase capacitor on the same line as is being analyzed, i.e., on phase X, has been shown. Two other connections are tested: 1) two capacitors are connected between phase Y and neutral and between phase Z and neutral, respectively, and 2) three capacitors are connected in a Wye configuration. All capacitors are 1-μF-film capacitors. The four capacitor connection cases are shown together in Fig. 16. Interestingly, the YZ case has an impact on the X phase. This likely results primarily from phase-to-phase interactions in the building's step-down transformer.

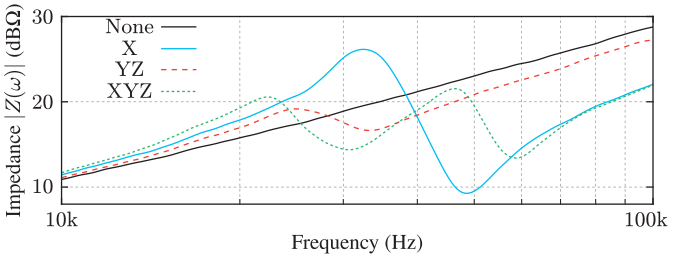

Fig. 16. Line impedance of the single-phase utility cable and electric utility with various phase to neutral capacitors connected.

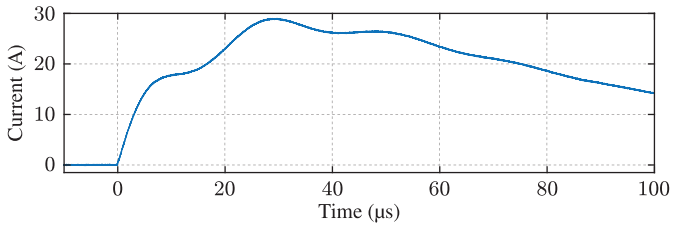

Fig. 17. Current inrush of an LED light at a 90° turn-on angle.

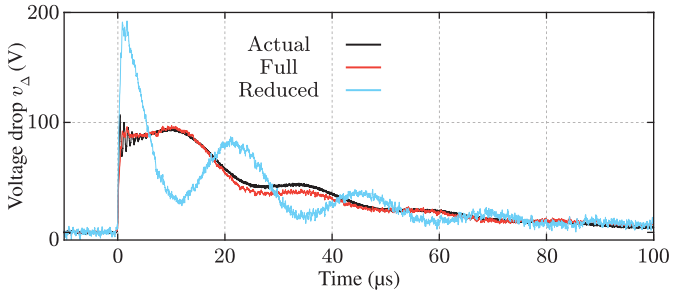

Fig. 18. Voltage disturbances for the LED light inrush transient. The actual result is shown along with the predictions based on the higher order (full) and reduced-order (R–L) line impedance models.

Phase-to-phase coupling by three-phase equipment may also play a role. The round-trip path through the transformer has more inductance and resistance, both lowering the frequency at which the impedance inflection occurs and decreasing its magnitude. The three-phase case introduces both a lower frequency interaction from phase Y and Z capacitors and a higher frequency interaction from the phase X capacitor. The differences between these interactions can be used to identify how a capacitive load is connected to the line.

The higher order line impedance model generated using the frequency spectrum approach improves the accuracy of power quality predictions. Based on the load current and the model of the line, the line voltage distortion can be estimated without direct measurement. With no other changes in the measurement setup, the incandescent bulb is again swapped with the same 5-W LED light used for Fig. 11. The single-phase utility cable and an additional 1-μF capacitor on phase X are also connected. Testing indicates that the load is a full bridge rectifier feeding into a large capacitor that is then connected to the LEDs.

A single-load transient was generated at a 90° turn-on angle, and the current in Fig. 17 was observed. A simulation passes this current through both the higher order "full" model and reduced-order R–L model to generate the voltage distortion prediction in Fig. 18. The actual voltage distortion, v_Δ, is also plotted. While the reduced-order model differs greatly from the actual result, the full model provides an excellent match. The initial ringing in the actual waveform comes from the high-frequency capacitance that was not included in the full model. Any other discrepancy between the waveforms is likely related to the nonlinear effects of the line. In particular, the skin effect will affect the model resistance parameters depending on the frequency characteristics of the current transient.

VII. Discussion

Overall, the NPIE approach has demonstrated more functionality and effectiveness than the PIE method for the purposes of the line-impedance characterization contemplated here. The ability to select the line impedance model from the generated plots has been proven useful and permitted an excellent fit to the case with additional line capacitance. Also, the generation of an impedance frequency spectrum makes this technique useful for PLC applications. Although the measurement became more difficult for turn-on angles near the zero crossings, a practical system would avoid these angles. The R–L model parameters are more consistent than obtained through the operator substitution method. With the NPIE approach, the excitation and subsequent model selection are clearer.

Line impedance characterization is a relevant topic for a variety of applications. Testing methodologies are often unnecessarily application-specific, e.g., in the sense of requiring or imposing a certain load. By using an inrush transient from any load to perturb the line, a large amount of information about the line can be gathered. This article presents a single device capable of both characterizing the R–L characteristics of the line and generating the line-impedance frequency spectrum using NPIE. The estimation easily extends to low frequencies while maintaining safe isolation from high voltages for the user. The single turn-on characteristic of the TRIACs limits the performance of the estimation as it limits the amount of high-frequency content that can be injected. An FET-based switch will offer the possibility of more complex test patterns within a single line cycle. More complex patterns offer interesting possibilities for more advanced system identification and impedance measurement.

References

[1] G. Hallak, C. Niess, and G. Bumiller, "Accurate low access impedance measurements with separated load impedance measurements on the power-line network," *IEEE Trans. Instrum. Meas.*, vol. 67, no. 10, pp. 2282–2293, Oct. 2018.

[2] G. Hallak and G. Bumiller, "Data rate optimization on PLC devices with current controller for low access impedance," in *Proc. Int. Symp. Power Line Commun. Appl. (ISPLC)*, Mar. 2016, pp. 144–149.

[3] G. Hallak and G. Bumiller, "Throughput optimization based on access impedance of PLC modems with limited power consumption," in *Proc. IEEE Global Commun. Conf.*, Dec. 2014, pp. 2960–2965.

[4] W. Beattie and S. Matthews, "Impedance measurement on distribution networks," in *Proc. 29th Universities Power Eng. Conf.*, Sep. 1994, pp. 117–120.

[5] S. Shaw, R. Lepard, and S. Leeb, "Desire: A power quality prediction system," in *Proc. 28th Annu. North Amer. Power Symp.*, Nov. 1996, pp. 581–586.

[6] S. R. Shaw, C. R. Laughman, S. B. Leeb, and R. F. Lepard, "A power quality prediction system," *IEEE Trans. Ind. Electron.*, vol. 47, no. 3, pp. 511–517, Jun. 2000.

[7] M. H. Sarul, "Line inductance measurement by using commutation time in line commutated converters," *Electr. Eng.*, vol. 91, no. 1, pp. 1–8, Jun. 2009.
[8] N. Ishigure, K. Matsui, and F. Ueda, "Development of an on-line impedance meter to measure the impedance of a distribution line," in *Proc. IEEE Int. Symp. Ind. Electron. Proc. (ISIE)*, vol. 1, Jun. 2001, pp. 549–554.
[9] K. Matsui, H. Kojima, M. Koyama, I. Yamamoto, F. Ueda, and H. Mori, "Some measurement techniques of distribution line impedance on hot-line," in *Proc. Eur. Conf. Power Electron. Appl.*, Apr. 2005, p. 8.
[10] M. Ciobotaru, R. Teodorescu, P. Rodriguez, A. Timbus, and F. Blaabjerg, "Online grid impedance estimation for single-phase grid-connected systems using PQ variations," in *Proc. IEEE Power Electron. Specialists Conf.*, Jun. 2007, pp. 2306–2312.
[11] M. Thomas, T. Martin, and J. C. Balda, "Design and error analysis of a digital line impedance meter," in *Proc. 30th Annu. Conf. IEEE Ind. Electron. Soc. (IECON)*, vol. 3, Nov. 2004, pp. 3066–3070.
[12] M. B. Harris, A. W. Kelley, J. P. Rhode, and M. E. Baran, "Instrumentation for measurement of line impedance," in *Proc. IEEE Appl. Power Electron. Conf. Exposit. (ASPEC)*, vol. 2, Feb. 1994, pp. 887–893.
[13] M. Sigle, W. Liu, and K. D. Karlsruhe, "On the impedance of the low-voltage distribution grid at frequencies up to 500 kHz," in *Proc. IEEE Int. Symp. Power Line Commun. Appl.*, Mar. 2012, pp. 30–34.
[14] G. Chu, J. Li, and W. Liu, "Narrow band power line channel characteristics for low voltage access network in China," in *Proc. IEEE 17th Int. Symp. Power Line Commun. Appl.*, Mar. 2013, pp. 297–302.
[15] S. Zhu, C. J. Kikkert, and N. Ertugrul, "A wide bandwidth, on-line impedance measurement method for power systems, based on PLC techniques," in *Proc. IEEE Int. Symp. Circuits Syst. (ISCAS)*, Jun. 2014, pp. 1167–1170.
[16] S. Zhu, C. J. Kikkert, and N. Ertugrul, "Software for control and calibration of an inductive shunt on-line impedance analyzer," in *Proc. IEEE Int. Symp. Power Line Commun. Appl. (ISPLC)*, Mar. 2015, pp. 53–58.
[17] C. J. Kikkert and S. Zhu, "Resistive shunt on-line impedance analyzer," in *Proc. Int. Symp. Power Line Commun. Appl. (ISPLC)*, Mar. 2016, pp. 150–155.
[18] E. K. Saathoff, Z. J. Pitcher, S. R. Shaw, and S. B. Leeb, "Inrush current testing," in *Proc. IEEE Appl. Power Electron. Conf. Exposit. (APEC)*, Mar. 2020, pp. 2319–2326.
[19] R. Johansson, *System Modeling and Identification*. Upper Saddle River, NJ, USA: Prentice-Hall, 1993.
[20] L. Ljung, *System Identification: Theory for the User*. Upper Saddle River, NJ, USA: Prentice-Hall, 1999.
[21] P. M. T. Broersen, "A comparison of transfer function estimators," *IEEE Trans. Instrum. Meas.*, vol. 44, no. 3, pp. 657–661, Jun. 1995.
[22] D. D. S. Mota, "Estimating the frequency response of an excitation system and synchronous generator: Sinusoidal disturbances versus empirical transfer function estimate," *IEEE Power Energy Technol. Syst. J.*, vol. 5, no. 2, pp. 27–34, Jun. 2018.
[23] P. Guillaume, I. Kollar, and R. Pintelon, "Statistical analysis of nonparametric transfer function estimates," *IEEE Trans. Instrum. Meas.*, vol. 45, no. 2, pp. 594–600, Apr. 1996.
[24] L. Van der Sluis, *Transients in Power Systems*. Hoboken, NJ, USA: Wiley, 2001.
[25] A. Greenwood, *Electrical Transients in Power Systems*. Hoboken, NJ, USA: Wiley, 1971.
[26] M. AbolhasaniJabali and M. H. Kazemi, "Estimation of inertia constant of iran power grid using the largest simulation model and PMU data," in *Proc. 24th Iranian Conf. Electr. Eng. (ICEE)*, May 2016, pp. 158–160.
[27] D. P. Chassin, Z. Huang, M. K. Donnelly, C. Hassler, E. Ramirez, and C. Ray, "Estimation of WECC system inertia using observed frequency transients," *IEEE Trans. Power Syst.*, vol. 20, no. 2, pp. 1190–1192, May 2005.
[28] H. Xue, M. Wang, R. Yang, and Y. Zhang, "Power system frequency estimation method in the presence of harmonics," *IEEE Trans. Instrum. Meas.*, vol. 65, no. 1, pp. 56–69, Jan. 2016.
[29] A. Radonjic, P. Sovilj, and V. Vujicic, "Stochastic measurement of power grid frequency using a two-bit A/D converter," *IEEE Trans. Instrum. Meas.*, vol. 63, no. 1, pp. 56–62, Jan. 2014.
[30] H. Ahmed, M. Bierhoff, and M. Benbouzid, "Multiple nonlinear harmonic oscillator-based frequency estimation for distorted grid voltage," *IEEE Trans. Instrum. Meas.*, vol. 69, no. 6, pp. 2817–2825, Jun. 2020.

Erik K. Saathoff (Graduate Student Member, IEEE) received the B.S. degree in electrical engineering with a minor in physics from the University of Illinois at Urbana–Champaign, Urbana, IL, USA, in 2018. He is currently pursuing the M.S. and Ph.D. degrees in electrical engineering and computer science with the Massachusetts Institute of Technology, Cambridge, MA, USA.

His research interests include high-performance power electronics, switched-capacitor converters, and system identification.

Steven R. Shaw (Senior Member, IEEE) received the Ph.D. degree in electrical engineering from the Massachusetts Institute of Technology, Cambridge, MA, USA, in 2000.

He is currently a Professor with the Department of Electrical and Computer Engineering, Montana State University, Bozeman, MT, USA. His research interests include system identification and controls, instrumentation, and energy conversion.

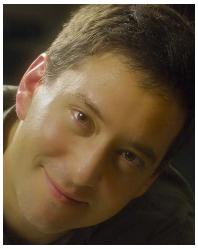

Steven B. Leeb (Fellow, IEEE) received the Doctoral degree from the Massachusetts Institute of Technology, Cambridge, MA, USA, in 1993.

He served as a Commissioned Officer in the USAF reserves, and he has been a member of the MIT Faculty, Department of Electrical Engineering and Computer Science, since 1993. He also holds a joint appointment in MIT's Department of Mechanical Engineering. He is the author or a coauthor of over 200 publications and holds 20 U.S. patents in the fields of electromechanics and power electronics.